JACS
JOURNAL OF THE AMERICAN CHEMICAL SOCIETY

Article

pubs.acs.org/JACS

An Unusual Peroxo Intermediate of the Arylamine Oxygenase of the Chloramphenicol Biosynthetic Pathway

Thomas M. Makris,[†,¶] Van V. Vu,[¶,‡] Katlyn K. Meier,[§] Anna J. Komor,[¶,‡] Brent S. Rivard,[†,¶] Eckard Münck,*[,§] Lawrence Que, Jr.,*[,¶,‡] and John D. Lipscomb*[,†,¶]

[†]Department of Biochemistry, Molecular Biology, and Biophysics, [¶]Center for Metals in Biocatalysis, and [‡]Department of Chemistry, University of Minnesota, Minneapolis, Minnesota 55455, United States

[§]Department of Chemistry, Carnegie Mellon University, Pittsburgh, Pennsylvania 15213, United States

Supporting Information

ABSTRACT: *Streptomyces venezuelae* CmlI catalyzes the six-electron oxygenation of the arylamine precursor of chloramphenicol in a nonribosomal peptide synthetase (NRPS)-based pathway to yield the nitroaryl group of the antibiotic. Optical, EPR, and Mössbauer studies show that the enzyme contains a nonheme dinuclear iron cluster. Addition of O_2 to the diferrous state of the cluster results in an exceptionally long-lived intermediate ($t_{1/2}$ = 3 h at 4 °C) that is assigned as a peroxodiferric species (CmlI-peroxo) based upon the observation of an $^{18}O_2$-sensitive resonance Raman (rR) vibration. CmlI-peroxo is spectroscopically distinct from the well characterized and commonly observed *cis*-μ-1,2-peroxo (μ-η^1:η^1) intermediates of nonheme diiron enzymes. Specifically, it exhibits a blue-shifted broad absorption band around 500 nm and a rR spectrum with a ν(O−O) that is at least 60 cm^{-1} lower in energy. Mössbauer studies of the peroxo state reveal a diferric cluster having iron sites with small quadrupole splittings and distinct isomer shifts (0.54 and 0.62 mm/s). Taken together, the spectroscopic comparisons clearly indicate that CmlI-peroxo does not have a μ-η^1:η^1-peroxo ligand; we propose that a μ-η^1:η^2-peroxo ligand accounts for its distinct spectroscopic properties. CmlI-peroxo reacts with a range of arylamine substrates by an apparent second-order process, indicating that CmlI-peroxo is the reactive species of the catalytic cycle. Efficient production of chloramphenicol from the free arylamine precursor suggests that CmlI catalyzes the ultimate step in the biosynthetic pathway and that the precursor is not bound to the NRPS during this step.

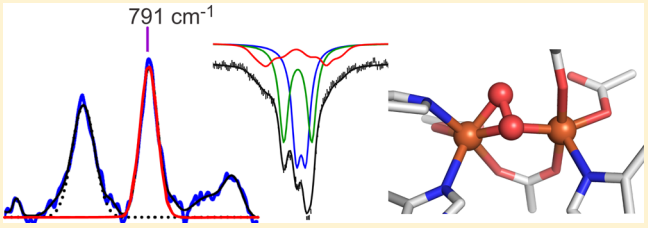

INTRODUCTION

Carboxylate-bridged diiron cluster-containing monooxygenases catalyze an extraordinary array of chemical reactions, including the oxidation of aliphatic C−H bonds for carbon utilization,[1] antibiotic biosynthesis,[2,3] the maturation of proteins involved in cell proliferation,[4] and the post-translational modification of tRNA,[5] among many others. Studies of oxygen activation in diiron hydroxylase enzymes and functional mimics have revealed that the most common mechanism for dioxygen activation in this class of enzymes involves the initial binding of O_2 to the reduced diferrous cluster, resulting in the formation of a peroxodiferric metal−oxygen adduct.[6−8] Subsequent to formation of this initial complex, the reactivities of diiron oxygenases diverge. In some cases, the peroxo intermediate is thought to directly participate in the oxidation of weak C−H bonds;[9] in others, it is known to undergo O−O bond cleavage to form a high-valent metal-oxo adduct that can transfer oxygen to inert hydrocarbons.[10−12] The peroxo intermediate is also the precursor of species involved in radical formation in ribonucleotide reductase (RNR)[13,14] and thought to be involved in desaturation reactions by fatty acid desaturases.[15] Therefore, studies of the electronic structures and reactivities of diiron-peroxo intermediates are of central importance in understanding catalysis by a large number of diverse biological systems.

The reactive nature of diferric-peroxo intermediates often prohibits accumulation to concentration levels that permit structural interrogation. As a result, a thorough spectroscopic and structural study that can successfully address the O_2 coordination mode has been limited to a handful of diiron enzymes in which the Fe_2O_2 unit is unusually long-lived. In each of these cases, including the D84E/W48F mutant of RNR,[8,16,17] fatty acid Δ^9 desaturase (Δ^9D),[15,18] and deoxyhypusine hydroxylase (hDOHH),[4] dioxygen has been shown to bridge the two iron atoms in a μ-η^1:η^1 coordination mode. Accordingly, the optical spectrum of the peroxodiferric intermediate in these enzymes has been shown to exhibit an intense (ε > 1000 M^{-1} cm^{-1}) charge-transfer band with λ_{max} between 600 and 700 nm, similar to intermediates observed in transient kinetic studies of methane monooxygenase[19] and biomimetic model complexes.[20−24]

Despite the uniformity of the dioxygen binding mode observed for the spectroscopically characterized peroxodiferric intermediates, the possibility of alternative coordination geometries has been raised based on the distinct spectroscopic properties, primarily optical and Mössbauer, observed in transient

Received: November 12, 2014
Published: January 6, 2015

DOI: 10.1021/ja511649n
J. Am. Chem. Soc. 2015, 137, 1608−1617

intermediates of toluene/*o*-xylene monooxygenase (ToMO),[25,26] *para*-aminobenzoate *N*-oxygenase (AurF),[27,28] aldehyde deformylating oxygenase (ADO),[29] and the ribonucleotide reductase variant W48A/Y122F.[30] In contrast to the canonical μ-η^1:η^1 peroxo intermediates, these diferric intermediates do not exhibit the optical signature band at ~700 nm and instead show either no apparent optical absorption (e.g., ToMO) or a weaker ($\varepsilon \leq 500\ M^{-1}\ cm^{-1}$) feature at shorter wavelength (450−500 nm; e.g., ADO, AurF, and RNR W48A/Y122F). Mössbauer spectroscopy similarly suggests that the O_2 binding mode of these species may indeed deviate from μ-η^1:η^1 coordination, as suggested by a significant decrease in quadrupole splitting ($\Delta E_Q \leq 0.7$ mm/sec) when compared to corresponding values ($\Delta E_Q > 1$ mm/sec) in peroxo intermediates that display the 700 nm band. Despite the marked discrepancy of the spectroscopic features of these peroxo intermediates versus those of the structurally characterized μ-η^1:η^1 peroxodiferric complexes, the direct demonstration of an alternative peroxo ligand geometry has not been obtained in any dinuclear iron enzyme. In contrast, a variety of alternative binding modes, including the μ-η^2:η^2 or μ-η^1:η^2, have been observed in dicopper cluster-containing enzymes and heteronuclear heme iron:copper model complexes, suggesting that they may also be found in diiron cluster-containing systems.[4,8,15,31−40]

Arylamine oxygenases are a recently characterized class of diiron oxygenases involved in the biosynthesis of a nitroaryl moiety in a number of antibiotic pathways, including aureothin[41,42] and chloramphenicol.[43,44] This enzyme family, exemplified by AurF from the aureothin biosynthetic pathway, has been shown to catalyze nitro group formation through the six-electron oxidation of an amine precursor. This process may involve intermediary hydroxylamino-, dihydroxylamino-, and nitroso-oxidation products, although only the hydroxylamino derivative has been shown to be metabolized when used as an initial substrate in the case of AurF.[28,42] Studies have now firmly established that AurF utilizes a diferrous cofactor to activate O_2 in a manner reminiscent of the bacterial multicomponent monooxygenase (BMM) superfamily.[3,27] The diiron active-site of AurF is structurally similar to those of the BMMs, including that of methane monooxygenase (MMO).[45,46] The most notable deviation in the primary ligation environment is the presence of an additional histidine ligand in AurF, which substitutes for a water ligand in MMO and other members of the superfamily.

Recent studies of AurF by Bollinger, Krebs, and colleagues have shown that the O_2 activation mechanism of arylamine oxygenases may permit an unprecedented opportunity to structurally characterize a diiron-peroxo intermediate with a unique O_2 coordination geometry.[27,28] Exposure of reduced AurF to dioxygen resulted in the accumulation of a diferric intermediate with substantial kinetic stability, enabling its spectroscopic characterization by stopped-flow and rapid-freeze-quench techniques. While these approaches did not allow the structural details of the AurF peroxo unit to be fully elucidated, the observed optical and Mössbauer spectroscopic properties of the presumptive oxygen-bound intermediate suggest that the coordination geometry may significantly differ from the commonly observed μ-η^1:η^1 mode.

CmlI is an arylamine oxygenase from the nonribosomal peptide synthetase (NRPS)-based chloramphenicol biosynthetic pathway of *Streptomyces venezuelae*.[44,47] It has a high sequence identity (37%) to AurF, and thus it was proposed to contain a diiron cluster. Accordingly, sequence alignments suggest that the diiron clusters of CmlI and AurF have conserved ligand structures. CmlI and a β-hydroxylase, CmlA, from the same pathway were recently recognized as the first diiron cluster-containing oxygenases to function in an NRPS pathway.[2] CmlI and CmlA serve to tailor the developing antibiotic by adding or converting functional groups. Conversion of the arylamine to the nitroaryl group by CmlI is essential for the biocidal activity of chloramphenicol.[48] The similar amino acid sequences and catalyzed reactions of CmlI and AurF suggest that they may be able to form similar reactive intermediates.[44] Here, we show definitively that CmlI contains a diiron cluster and forms a hyperstable peroxo intermediate that can be spectroscopically characterized in solution as well as in frozen media. Using a combination of UV−vis, Mössbauer, and resonance Raman spectroscopies, we demonstrate that the diiron arylamine oxygenase generates a peroxodiferric intermediate with a geometry that has not been previously described in the nonheme iron family. Moreover, transient kinetic absorption and product identification studies suggest that the unique peroxo intermediate is the reactive species in the oxygenation of arylamine substrates. These studies directly demonstrate the role of CmlI in chloramphenicol biosynthesis.

RESULTS

Cloning, Overexpression, and Metal Center of CmlI.

The arylamine oxygenase, CmlI, catalyzes the reaction shown in the inset of Figure 1 to yield chloramphenicol. The enzyme was

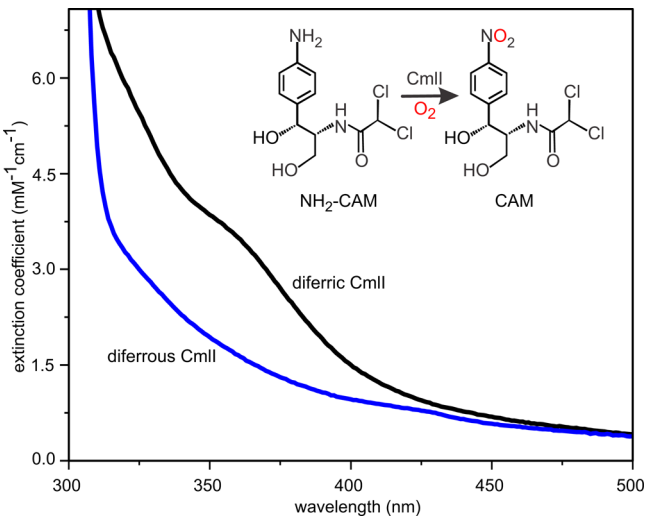

Figure 1. Optical absorption spectrum of resting CmlI (black trace) and dithionite reduced CmlI (blue trace). Buffer: 50 mM Bicine at pH 9.0, 25 °C. Inset: Reaction catalyzed by CmlI. At least one and probably both oxygens in the nitro group derive from O_2. The reaction is a net six-electron oxidation of the amine function, but the stoichiometries of O_2 utilization and electrons required during the reaction to activate O_2 are controversial. Abbreviations: NH_2-CAM, D-*threo*-1-(4-aminophenyl)-2-dichloroacetylamino-1,3-propanediol; CAM, chloramphenicol.

cloned from *S. venezuelae* genomic DNA of the chloramphenicol biosynthesis cluster, overexpressed in *E. coli*, and purified to homogeneity as described in Materials and Methods in the Supporting Information. The enzyme as isolated from M9 minimal media with exogenously added iron contained 2.1 ± 0.1 irons per monomer. The optical spectrum showed an intense chromophore at 375 nm ($\varepsilon \approx 2700\ M^{-1}\ cm^{-1}$) (Figure 1, black

DOI: 10.1021/ja511649n
J. Am. Chem. Soc. 2015, 137, 1608−1617

trace). Anaerobic reduction of the metal center with sodium dithionite required two reducing equivalents and resulted in a weak, featureless spectrum in the visible (Figure 1, blue trace). The resting and fully reduced forms of the enzyme are EPR silent at X band. However, the partially reduced enzyme exhibits a pH-dependent EPR spectrum (Figure S1), with the principal g-values below $g = 2$, a characteristic feature of an $S = 1/2$ ground-state species from an antiferromagnetically coupled $Fe^{III}Fe^{II}$ cluster. The metal quantification and the spectral characteristics of the oxidized enzyme are consistent with a dinuclear iron cluster in which the irons are bridged by an oxo ligand (see e.g., ref 2).

Mössbauer Characterization of CmlI. Mössbauer spectra of CmlI at pH 6.5, 7.5, and 9.0 (Figures 2, S2, and S3) indicate

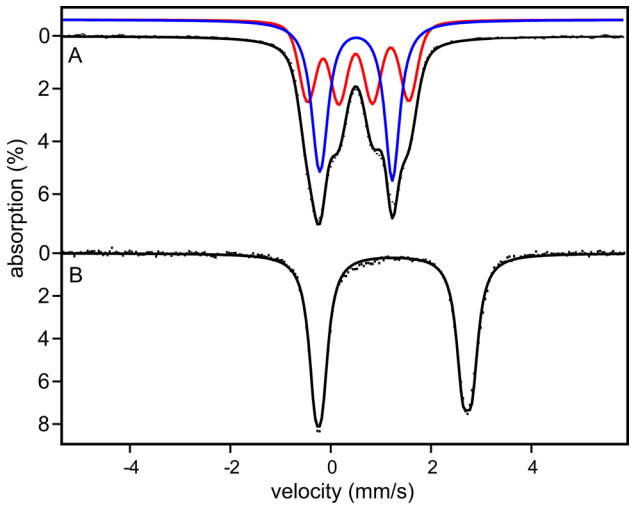

Figure 2. 4.2 K Mössbauer spectra of (A) as-isolated CmlI and (B) dithionite reduced CmlI. Spectra were obtained in the absence of an applied magnetic field ($B = 0$). Samples were prepared in Bicine buffer at pH 9.0. Solid black line in (A) is a spectral simulation assuming four quadrupole doublets of essentially equal intensity; parameters are listed in Table 1. The red line shows subspectra of nested doublets 1 and 4, while the blue line represents the superposition of the (similar) doublets 2 and 3. The sum of the red and blue lines yields the black curve. (B) The solid black line drawn through the experimental data of diferrous CmlI is a spectral simulation for two similar doublets using the parameters listed in Table 1.

that the protein contains a diiron center, in accord with the expectations based on the sequence similarities between CmlI and AurF. The spectra of diferric CmlI depend sensitively on the pH in ways we do not yet understand; the pH dependence is more complicated than that of a simple interconversion between two forms of the diiron cluster. The studies reported here focus on reduced CmlI and a reaction cycle intermediate at pH 9.0 in Bicine buffer, and so the following spectral analysis pertains to the enzyme under those conditions.

The 4.2 K Mössbauer spectra of as-isolated and dithionite reduced CmlI are shown in Figures 2 and S2–S4. A summary of all fitting parameters is given in Table 1. The spectrum of as-isolated CmlI at pH 9.0 (Figure 2A) is best described as a superposition of four quadrupole doublets, each having an isomer shift of $\delta \sim 0.50$–0.55 mm/sec that is characteristic of high-spin Fe^{III}. The observation of quadrupole doublets at 4.2 K (rather than spectra exhibiting paramagnetic hyperfine structure as typically observed for mononuclear Fe^{III} complexes) suggests exchange coupled pairs of iron atoms, in accord with the

Table 1. Quadrupole Splittings and Isomer Shifts for As-Purified, Dithionite-Reduced, and Oxygenated Forms of CmlI

			δ (mm/sec)	ΔE_Q (mm/sec)	area (%)
oxidized	cluster form 1[a]	doublet 1	0.55	2.02	~44
		doublet 4	0.50	0.64	
	cluster form 2[a]	doublet 2	0.50	1.48	~56
		doublet 3	0.52	1.40	
reduced		site 1	1.25	3.13	50
		site 2	1.23	2.80	50
oxygenated		site a	0.62	−0.23[b]	50[c]
		site b	0.54	−0.68[b]	50[c]

[a]We have assigned doublets 1 and 4, somewhat arbitrarily, to one cluster form and doublets 2 and 3 to a second cluster form. Given the uncertainties in line shapes, which affect the percentages, other pair combinations are possible. [b]Signs of ΔE_Q were determined from the 4.2 K spectrum taken at $B = 75$ kG. [c]Represents spectral contribution after removing 22% of oxidized pH 9 CmlI from the spectrum.

observations reported for numerous diiron proteins. The black line in Figure 2A represents the sum of the four doublets. The red line shows the sum of the nested doublets 1 and 4, while the blue line represents the sum of the (unresolved) doublets 2 and 3. The decomposition of the spectrum into four doublets is supported by the Fourier transform treated spectrum shown in Figure S2. Such treatments[49−51] increase the resolution of the spectrum by removing the line width contribution of the ^{57}Co radiation source, a procedure that sharpens the absorption lines by roughly a factor of two. In Figure S2 the presence of three doublets is quite apparent, and it is also apparent that one of the three doublets is broader and more intense and thus must be composed of two similar subspecies. The observation of four doublets shows that the oxidized enzyme can stabilize at least two cluster forms in which the two irons of each cluster type reside in different environments. The 4.2 K Mössbauer spectra obtained at pH 6.5 and 7.5 (shown in Figure S3) are not related to that of the pH 9.0 form by a simple redistribution of the intensities of doublet pairs. Following the doublet pattern to lower pH did not yield the desired pairings, as ΔE_Q changes were observed that affect a single site in a cluster (as might be expected for a carboxylate changing from monodentate to bidentate coordination, or protonation of a monodentate carboxylate) as well as changes affecting both iron sites of a cluster (such as a change involving a bridging ligand). In Table 1 the doublets are enumerated in order of descending quadrupole splittings, ΔE_Q. There is no ambiguity in the assignment of the lines of doublets 1 and 4, as combining lines assigned to these doublets with those of doublets 2 and 3 would yield unreasonable pairs of δ values. Observation of iron clusters with similar isomer shifts but different quadrupole splitting suggests that while the two irons belong to the same cluster, they experience different local environments. In contrast to the pairing of doublets 1 and 4, combining the four lines of the similar doublets 2 and 3 into a non-nested pair would yield two doublets with parameters similar to doublets 2 and 3. Presently, we do not see an obvious way of combining the four doublets uniquely into two cluster types. Cluster form 1, comprising doublets 1 and 4, represents ca. 44% of the Fe in the sample, whereas cluster form 2 accounts for 56%. Interestingly, the pH 7.5 spectrum of CmlI resembles the pH 7.5 spectrum of AurF reported by Krebs and co-workers (overlay shown in Figure S4).[27]

DOI: 10.1021/ja511649n
J. Am. Chem. Soc. 2015, 137, 1608−1617

Figure 2B shows a zero-field Mössbauer spectrum of dithionite-reduced CmlI. The spectrum consists of a doublet with parameters typical of high-spin Fe^{II}. Spectral simulations indicate that the spectrum is a superposition of two overlapping doublets with $\Delta E_Q(1)$ = 3.13 mm/s, $\delta(1)$ = 1.25 mm/s and $\Delta E_Q(2)$ = 2.80 mm/s, $\delta(2)$ = 1.23 mm/s, parameters quite similar to the ΔE_Q = 3.06 mm/s, $\delta(2)$ = 1.24 mm/s reported for diferrous AurF.[27] Our simulations require a Lorentzian line width of 0.30 mm/s full width at half-maximum (attempts to simulate the spectrum with one doublet, while using different widths for the high-and low-energy features did not produce good matches in the wings of the high-energy line). The above choice of parameters results when the nested combination of the two doublets is chosen; the non-nested combination would yield the less plausible parameter set with $\delta(1)$ = 1.16 mm/s and $\delta(2)$ = 1.33 mm/s. In contrast to the diferric state, only one cluster form, with two slightly inequivalent sites, seems to be present in the diferrous state. The presence of only one cluster form in the reduced state of the protein, rather than two as observed in the oxidized state, would not be surprising as diiron clusters generally experience considerable ligand changes and rearrangements upon reduction, such as loss of an oxo bridge and carboxylate shifts.[52−55]

A Long-Lived Intermediate is Formed Upon Exposure of Reduced CmlI to Dioxygen. The addition of excess dioxygen to the dithionite-reduced, anaerobic enzyme results in the appearance of a broad new optical absorption band at approximately 500 nm ($\varepsilon \approx 500\ M^{-1}\ cm^{-1}$ per diiron cluster) (Figure 3, red trace). The spectrum of this species is similar to

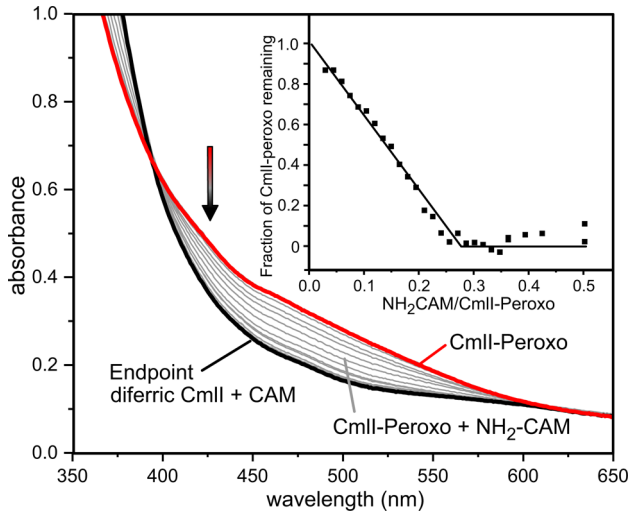

Figure 3. Reaction of CmlI-peroxo with NH_2-CAM. CmlI-peroxo (red trace) was formed by exposure of stoichiometrically reduced diferrous CmlI to O_2. Aliquots of NH_2-CAM (~0.05 equiv) were added, and the spectrum scanned (gray traces, only selected traces are shown for clarity). At the end of the titration, the spectrum of the resting diferric enzyme is restored (black trace). Buffer: 50 mM Bicine, pH 9, 4 °C. Inset: Fraction of CmlI-peroxo remaining at each point during the titration plotted as a function of NH_2-CAM equivalents added.

that reported for the proposed peroxo intermediate of AurF.[27] Extended incubation of this likely CmlI-peroxo species (this assignment is made directly below) leads to the slow restoration of a spectrum indistinguishable from that of the resting diferric enzyme. The stability of the 500 nm absorbing species was determined in transient kinetic experiments over a

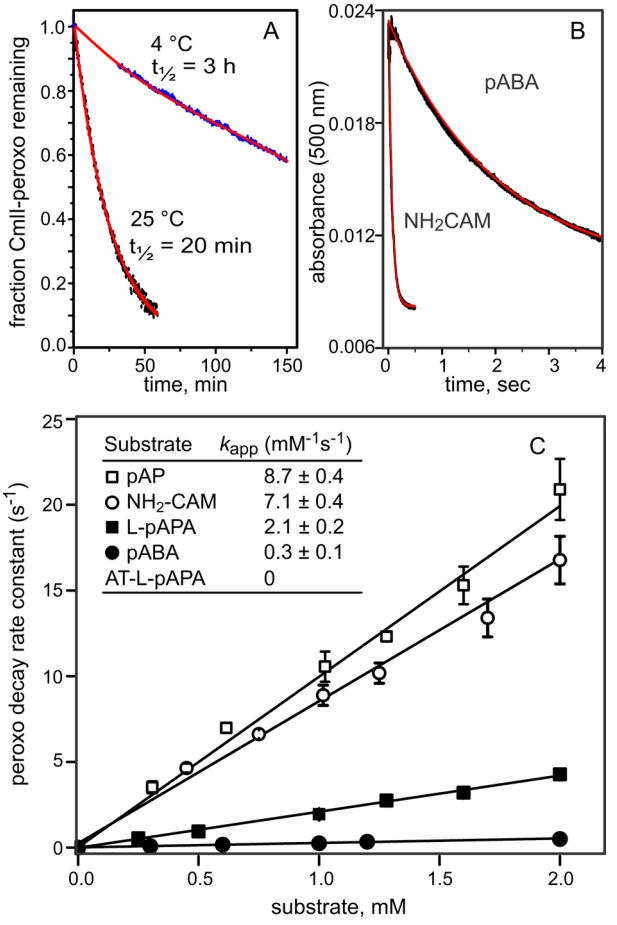

Figure 4. Single turnover reaction of CmlI-peroxo with substrates. (A) Autodecay time course (filled ovals) for reaction of 600 μM preformed CmlI-peroxo at 4 or 25 °C. A single exponential fit (red) is shown superimposed on the data. (B) Single turnover time course for reaction of 50 μM preformed CmlI-peroxo with 1 mM of the substrate shown (black). A single-exponential fit (red) is shown superimposed on the data. (C) Plot of the apparent first-order CmlI-peroxo decay rate constant for the reaction of 50 μM diferrous CmlI with 850 μM O_2 and the concentration of the substrate shown (all concentrations after mixing). Inset: Apparent second-order rate constants calculated from the slopes of the plots in the main figure. Buffer: 50 mM Bicine at pH 9.0, 4 °C except where noted. Abbreviations: pAP, *para*-aminophenol; L-pAPA, L-*para*-aminophenylalanine; pABA, *para*-aminobenzoate; AT-L-pAPA, L-pAPA loaded covalently onto the thiolation domain of a CmlP (the NRPS) construct consisting of only the adenylation and thiolation domains. No reaction beyond autodecay was detected when using AT-L-pAPA.

range of temperatures. The time course for its decay could be fit by a single exponential expression at all temperatures examined (Figure 4A). The oxygenated form of CmlI demonstrates extraordinary stability, with measured half-lives of 20 min and 3 h at 25 and 4 °C, respectively. The stability of this intermediate in CmlI is substantially greater than that of the similar intermediate observed for AurF, ($t_{1/2} \approx 7$ min at 20 °C),[27] which facilitates studies of its reactivity and structure.

Reactivity of the CmlI-Peroxo Intermediate. Addition of the chloramphenicol precursor D-*threo*-1-(4-aminophenyl)-2-dichloroacetylamino-1,3-propanediol (NH_2-CAM) to the CmlI-peroxo species resulted in a rapid loss of the optical features of the intermediate (Figure 4B). The acceleration of the decay of the intermediate, at 4 °C, is approximately

DOI: 10.1021/ja511649n
J. Am. Chem. Soc. 2015, 137, 1608−1617

100,000-fold when using 1 mM NH_2-CAM. Titration of CmlI-peroxo species with aliquots of NH_2-CAM resulted in the restoration of the spectrum of the resting enzyme (Figure 3, gray traces leading to the black trace). Extraction of the reaction solution and analysis by HPLC and extracted ion mass spec showed that the product of the reaction is chloramphenicol (Figure S5). Chloramphenicol was also shown to be the product from this substrate in previous continuous turnover reactions of CmlI.[44] A plot of the disappearance of CmlI-peroxo vs the NH_2-CAM equivalents added (Figure 3, inset) shows that approximately three CmlI-peroxo complexes are consumed for each chloramphenicol formed. A similar stoichiometry was reported for the conversion *para*-aminobenzoate (pABA) to *para*-nitrobenzoate (pNB) by AurF, although a later study cast doubt on this stoichiometry.[27,28]

CmlI-Peroxo Appears to React Directly with Substrates. The exceptionally long lifetime of the CmlI-peroxo allows the formation of the intermediate before transfer to a stopped-flow syringe, so that the reaction with NH_2-CAM and a variety of adventitious substrates can be easily observed (Figure 4B,C). The decay time course is fit well by a single exponential for each substrate, consistent with a single-step reaction or a rate-limiting reaction followed by much more rapid reactions to form product. The reciprocal relaxation time (RRT) for the decay of the CmlI-peroxo depends on both the concentration and type of substrate provided as shown in Figure 4C. It is interesting that the plot of the RRT versus the substrate concentration is linear extrapolating to zero for each substrate when the substrates are supplied in large excess. This suggests that the reaction is irreversible, and thus, the observed RRT is the pseudo-first-order rate constant for the reaction. The linear dependence of the pseudo-first-order rate constant is surprising, as it implies that the reaction of CmlI-peroxo with amine substrates occurs as a second-order process without formation of a kinetically significant enzyme−substrate complex. To our knowledge, the only diiron enzyme intermediate that behaves kinetically in this way is the MMO bis-μ-oxo Fe^{IV} Fe^{IV} intermediate Compound Q.[10] However, slow, soluble alternative substrates for Compound Q reactions showed hyperbolic substrate concentration dependence, suggesting that a high K_m complex is, in fact, formed.[56] In the case of CmlI, no deviation from linearity was observed at concentrations up to 50 mM for the most soluble substrates tested (Figure S6). Apparent second-order rate constants for the CmlI-peroxo reaction with arylamine substrates are shown in Figure 4C, inset. Interestingly, the chloramphenicol precursor L-*para*-aminophenylalanine (L-pAPA) is not a substrate when bound to the NRPS for the system, CmlP, truncated to the adenylation and thiolation domains.

Characterization of the Oxygenated Intermediate by Mössbauer Spectroscopy. The exceptional stability of the oxygenated CmlI intermediate enables its spectroscopic interrogation at enzyme and O_2 concentrations that surpass those normally obtained in rapid mixing experiments, as the intermediate can be prepared quite simply through the gradual addition of gaseous O_2 to the reduced enzyme at 4 °C. A 2 mM solution of dithionite-reduced CmlI, at pH 9.0, was gently oxygenated with a stream of O_2 gas at 4 °C for 10 min and subsequently frozen in liquid nitrogen.

As shown in Figure 5A the 4.2 K zero-field Mössbauer spectrum of this sample is quite different from those of the resting and dithionite-reduced enzyme. The majority component, assigned to diferric CmlI-peroxo, comprises two nested

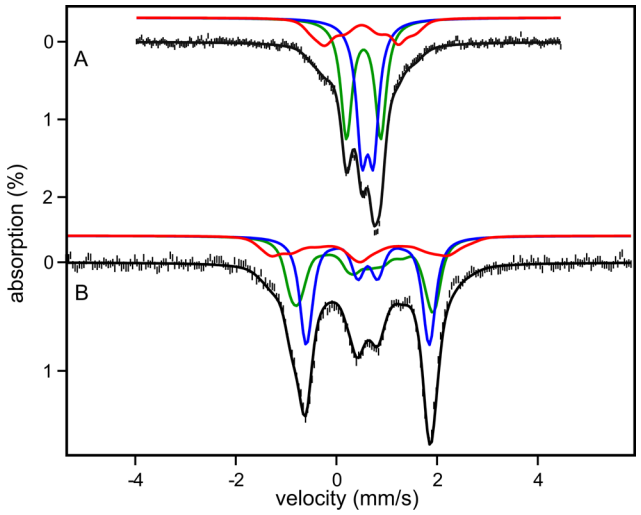

Figure 5. 4.2 K Mössbauer spectra of the oxygenated CmlI. (A) Zero-field spectrum. The green and blue curves are spectral simulations for sites *a* and *b* of the major (>80%) peroxo species. The red curves outline the 20% contribution of a diferric contaminant, assumed to be the pH 9 species of Figure 2A. (B) Spectrum of the same sample recorded in a parallel applied field of 7.5 T. The blue and green lines are spectral simulations of the diiron(III) peroxo components. The remaining (red) simulated spectrum, accounting for roughly 20% of the experimental spectrum, was well approximated with δ and ΔE_Q parameters of pH 9 as-isolated diferric CmlI.

doublets of equal intensity that account ca. 80% of the iron in the sample. Doublet *a* (simulated blue curve) has ΔE_Q (*a*) = −0.23(1) mm/s, δ (a) = 0.62(1) mm/s, while doublet *b* (green line) has ΔE_Q (*b*) = −0.68(2) mm/s, δ (*b*) = 0.54(1) mm/s. The two doublets are superimposed on a minority species that contributes the shoulders at +1.5 and −0.5 mm/s Doppler velocity. This spectral component seems to comprise the four doublets observed for the diferric pH 9.0 CmlI of Figure 2A, and it accounts for ≈20% of the iron in the sample. Given the observed rate constant of ≈0.005 min^{-1} for the decay of the CmlI-peroxo, at 4 °C, about 10% diferric CmlI is expected at the time the sample was frozen. The remainder, if any, probably derives from incomplete reduction. Subtracting the diferric species (indicated by the red line) results in the removal of the shoulders and yields two doublets *a* and *b*. The ΔE_Q and δ parameters listed in Table 2 were obtained by assigning the four lines to two nested doublets; the non-nested choice would yield ΔE_Q (*a*′) = −0.37 mm/s, δ (*a*′) = 0.69 mm/s and ΔE_Q (*b*′) = −0.54 mm/s, δ (*b*′) = 0.46 mm/s, a combination with less plausible δ values in our opinion. Krebs and coworkers have observed a very similar species for AurF-peroxo (see Table 2, Figure S1, and caption of ref 28). It is worth noting that the two doublets of $Fe^{III}Fe^{III}$ CmlI-peroxo (and AurF-peroxo) have quite different δ values, a situation similar to that reported by Chavez et al. for the intermediate obtained by exposing the diiron(II) "paddlewheel" complexes of sterically hindered $ArCO_2^-$ ligands to O_2.[57] We address this observation below.

The $Fe^{III}Fe^{III}$ CmlI-peroxo complex exhibits quadrupole doublets at 4.2 K, which suggests an exchange coupled, high-spin diferric system for which the local spins $S_1 = S_2 = 5/2$ are antiferromagnetically aligned. The 7.5 T spectrum of Figure 5B can be simulated under the assumption that the ^{57}Fe nuclei experience only the applied field, i.e., the ground state of $Fe^{III}Fe^{III}$ CmlI-peroxo has a cluster spin $S = 0$. By recording

DOI: 10.1021/ja511649n
J. Am. Chem. Soc. 2015, 137, 1608−1617

Table 2. Spectroscopic Parameters of Peroxodiiron(III) Intermediates Observed in Dinuclear Iron Enzymes

O_2 adducts of diiron(II) enzymes	λ_{max} (nm) ε (M^{-1} cm^{-1})	δ (mm/s)	ΔE_Q (mm/s)	J (cm^{-1})	ν(O−O) (cm^{-1}) Δ(^{16}O-^{18}O)	peroxo binding mode	refs
hDOHH	630 (1500)	0.55, 0.58[a]	1.16, 0.88	50−70	855 (44)	μ-OH-μ-η^1:η^1	4
MMOH	725 (1800)	0.69	1.55			μ-η^1:η^1	12,51,58
D84E R2	700 (1500)	0.63	1.58	50	868 (46)	μ-η^1:η^1	8,14,16,17,59
frog M ferritin	650 (1000)	0.62	1.08	70	851 (−51)	μ-η^1:η^1	33,59,60
stearoyl-ACP Δ^9 desaturase	700 (1100)	0.68,0.64	1.90, 1.06		898 (−54)	μ-η^1:η^1	15,18
ToMO	no visible band	0.55	0.67				25
W48A/Y122F R2	500 (1500)	0.52, 0.45	0.55, 1.53			–	30
ADO	450 (1200)	0.48, 0.49	0.55, 1.23			–	29
AurF	500 (500)	0.61, 0.55	0.35, 0.74[b]			–	27
CmlI	500 (500)	0.62, 0.54	−0.23, −0.68[b]	≥20	791 (43)	μ-η^1:η^2	this work

[a]Alternatively, the Mössbauer data can be assigned, less plausibly, as a non-nested pair of doublets with parameters δ = 0.49, 0.63 mm/s and ΔE_Q = 1.05, 0.99 mm/s [b]Values for assumption of nested doublets; signs of ΔE_Q unknown.

applied field Mössbauer spectra between 20 and 100 K one can often measure the exchange coupling constant J. This technique works well for $J \leq 120$ cm^{-1} provided the electronic spin relaxes either fast or slow compared to the nuclear precession frequencies. At intermediate relaxation rates, however, the spectra are broad, and an analysis of such spectra, to our knowledge, has not yet been reported for a diferric system. Unfortunately, this situation applies to the $Fe^{III}Fe^{III}$ peroxo species of CmlI. The exchange Hamiltonian $\mathcal{H} = JS_1 \cdot S_2$ produces a spin ladder S = 0, 1, ..., 5 for which the first excited state, the S = 1 multiplet, has energy J. For $J \leq 20$ cm^{-1} a field of 7.5 T would mix the $M_S = \pm 1$ sublevels of the S = 1 multiplet into the ground state, and this mixing would readily be detected in the 4.2 K spectrum. As there is no evidence for such mixing in the spectrum of Figure 5B, we conclude that $J_{peroxo} > 20$ cm^{-1}.

Resonance Raman Spectroscopy of the CmlI Oxygenated Intermediate. Resonance Raman spectroscopy can be used to demonstrate the presence of a peroxo ligand bound to the diiron(III) site and provides a means to evaluate the cluster structure of the intermediate absorbing at 500 nm. Figure 6 shows the resonance Raman spectra obtained by 488 nm excitation of CmlI-peroxo samples prepared with different oxygen isotopes as well as the spectrum of a sample in which the intermediate was allowed to decay (full spectral range is shown in Figure S7). The spectrum of the $^{16}O_2$ adduct (trace A) exhibits a peak at 791 cm^{-1} that slowly decays over 7 h at 0 °C (trace D), matching the observed kinetics at 500 nm described above. The spectrum of the $^{18}O_2$ adduct (97% enrichment) (trace B) shows a downshift of the 791 cm^{-1} peak to 748 cm^{-1}. The observed 43 cm^{-1} downshift of the 791 cm^{-1} peak almost matches the value calculated by Hooke's law for a diatomic O−O oscillator (−45 cm^{-1}). A mixed-isotope labeling experiment (trace C) shows the appearance of a band at 768 cm^{-1}, halfway between those of the $^{16}O_2$- and the $^{18}O_2$-derived samples, demonstrating a vibrational mode that must involve both atoms of the added O_2 and cannot arise from other possible band assignments such as ν(Fe=O) or ν_{asym}(Fe−O−Fe) modes, which involve only one oxygen atom. Taken together, these observations confirm that this ~800 cm^{-1} feature arises from a peroxo moiety. (No $^{18}O_2$-sensitive vibration was observed in the 500 cm^{-1} region where the ν(Fe−O) mode would typically be found.) A perusal of Table 2 shows that CmlI-peroxo exhibits a ν(O−O) feature that is at least 60 cm^{-1} lower in frequency than observed for any other enzyme peroxodiiron(III) intermediate reported to date. Taken together, the Mössbauer and resonance Raman results point to an as yet unobserved structure for a peroxo intermediate of a nonheme diiron enzyme.

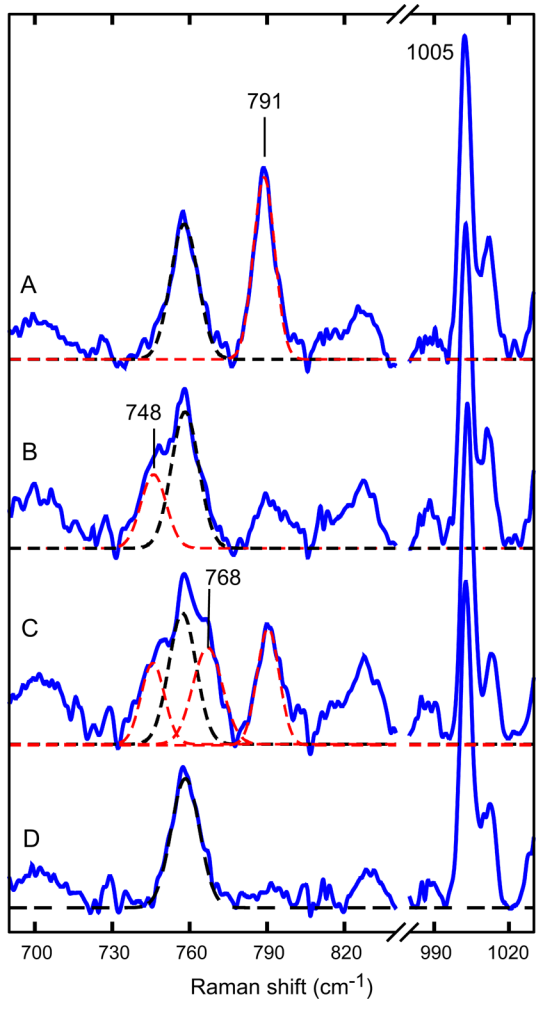

Figure 6. Resonance Raman spectra of oxygenated CmlI, pH 9.0, prepared with (A) $^{16}O_2$, (B) $^{18}O_2$, (C) mixed-labeled O_2, and (D) a sample after prolonged incubation. Spectra were obtained with 200−300 mW laser power and subjected to two-point baseline subtraction. No smoothing was required. Spectra were aligned and normalized using the sharp peak at 1005 cm^{-1} that arises from phenylalanine residues of the protein. Dashed lines represent Gaussian fits to the peaks of interest.

DOI: 10.1021/ja511649n
J. Am. Chem. Soc. 2015, 137, 1608−1617

DISCUSSION

It is shown here that CmlI-peroxo converts the arylamine precursor to chloramphenicol to the nitroaryl group of the active antibiotic. The metal center of CmlI is characterized as a diiron cluster that stabilizes an exceptionally long-lived peroxo intermediate. This intermediate appears to react directly with its substrate at physiologically relevant concentrations, suggesting that it is the reactive intermediate in the CmlI reaction cycle. It is noteworthy that CmlI-peroxo does not carry out the aliphatic or aromatic hydroxylations reactions reported for other diiron enzymes, and the latter enzymes do not carry out arylamine oxygenation.[7,9,10,25,27,28,61] The factors affecting stability of the diiron-peroxo intermediates and their substrate reactivity are largely unknown. Our kinetic and spectroscopic studies of CmlI-peroxo suggest that the unusual stability and substrate reactivity may result from formation of a previously uncharacterized peroxo structure. The bases for this conclusion are discussed here.

Nature of the CmlI-Peroxo Intermediate. The Mössbauer spectra of the diferric states of CmlI show that at least two cluster forms are present at each pH studied and that each cluster form has inequivalent Fe^{III} sites to yield four quadrupole doublets. These various forms occur in different ratios depending on conditions such as pH; at pH 9 two cluster forms in an approximate 1:1 ratio are present. The pH 9 Mössbauer spectrum of diferrous CmlI exhibits two similar, but unresolved, quadrupole doublets with ΔE_Q = 3.13 and 2.80 mm/s. For the closely related diferrous form of AurF (measured at pH 7.5) one broad quadrupole doublet was observed, with a ΔE_Q (= 3.06 mm/s) that is in between the ΔE_Q values determined here. These observations seem to suggest that the reduced enzymes contain just one cluster form, with indistinguishable sites in AurF and slightly different sites in CmlI, although what is known about the diiron cluster structure (two His ligands bound to one iron and one to the other, see Figure 7) suggests that strict equivalence is ruled out.

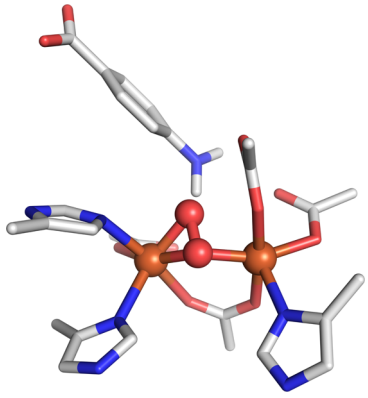

Figure 7. Proposed structure of CmlI-peroxo built from the active site coordinates of oxidized AurF-*para*-nitrobenzoate complex (3CHT). An oxygen atom was introduced to convert the oxo bridge into a μ-η^1:η^2-peroxo bridge. Fe, O, C, N, and H atoms are shown in orange, red, dark gray, blue, and light gray, respectively.

In contrast, the peroxo adducts of both CmlI and AurF exhibit a Mössbauer spectrum containing two equally intense quadrupole doublets, suggesting the presence of one cluster type with inequivalent Fe^{III} sites. (An interpretation that the two doublets represent two cluster forms, each with equivalent sites, seems contrived as each cluster would be required to have equivalent ferric sites that differ in isomer shift from those in the other cluster.) As pointed out above, the CmlI-peroxo cluster contains two antiferromagnetically coupled Fe^{III} sites; analysis of the 7.5 T spectrum of Figure 5 shows that $J > 20$ cm^{-1} (in the $\mathcal{H}_{exch} = J\, S_1 \cdot S_2$ convention).

The unusually low ν(O−O) frequency associated with the CmlI-peroxo intermediate suggests a peroxo binding mode not yet recognized within the family of dioxygen activating diiron enzymes. The four other peroxo intermediates of diiron enzymes characterized thus far by resonance Raman spectroscopy (Table 2) exhibit ν(O−O) frequencies in the range of 851−898 cm^{-1} and have been assigned to have μ-η^1:η^1 binding modes. The ν(O−O) frequencies of these complexes are at least 60 cm^{-1} higher than the 791 cm^{-1} value for CmlI-peroxo. Indeed, most synthetic diiron(III)-peroxo complexes described to date have μ-η^1:η^1 binding modes and exhibit the higher frequencies as well (Table 3).[20−24,34] The only potential exception to this generalization among diiron(III)-peroxo complexes is the O_2 adduct reported by Chavez et al.,[57] which has a ν(O−O) frequency at 822 cm^{-1}. This synthetic adduct also has a diferric cluster with relatively weak antiferromagnetic coupling ($J \sim 30$ cm^{-1}) and exhibits two doublets with distinct isomer shift values that are similar to those found for CmlI-peroxo. Unfortunately, there is no structural information available for this adduct.

Lower ν(O−O) frequencies are more typically observed for mononuclear (η^2-peroxo)iron(III) complexes (812−827 cm^{-1}; see Table 3). Even lower ν(O−O) frequencies (746−813 cm^{-1}) are found for a small subset of heterodinuclear complexes that consist of an (η^2-peroxo)iron(III) center having a second metal ion bound to the peroxo ligand to give rise to either a μ-η^2:η^2- or a μ-η^1:η^2-peroxo bridge. The first examples of such complexes featured a Cu^{II} as the second metal ion,[62,63] so the decrease in ν(O−O) could be attributed to an effect of the redox-active Cu^{II}, as previously observed in Cu^{II}_2(μ-η^2:η^2-peroxo) complexes.[64] However, more recently reported examples with redox-inactive Sc^{III} or Y^{III} as the second metal ion[65,66] also have lower ν(O−O) frequencies (but not as low as the dicopper complexes), so electron transfer from the second metal ion to the bound peroxo ligand is not required to lower the frequency of the side-on bound peroxo ligand. The fact that the ν(O−O) of CmlI-peroxo is observed at 791 cm^{-1} raises the strong possibility that its peroxo ligand may be bound in either the μ-η^2:η^2 or μ-η^1:η^2 bridging mode. Of these two modes, we favor the μ-η^1:η^2 bridging for the following reason: Site *a* has a substantially larger isomer shift (δ = 0.62(1) mm/s) than site *b* (δ = 0.54(1) mm/s), the latter value being associated with a more typical of high-spin ferric center. Mononuclear complexes with side-on bound peroxo groups generally have δ values between 0.58 and 0.67 mm/s (see Table 3), which suggests that site *a* of CmlI-peroxo could have a side-on peroxo ligand.

Figure 7 illustrates the proposed μ-η^1:η^2-peroxo binding mode for the CmlI active site, which was modeled by introducing an O atom to the oxo bridge between the iron atoms in the crystal structure of AurF-product complex (3CHT). It is not clear what factors cause this diiron active site to form an O_2-adduct distinct from the other four diiron enzyme O_2-adducts that have been characterized by resonance Raman spectroscopy. Perhaps the presumed third His ligand, deduced by comparison with the sequence of the structurally characterized AurF, promotes the shift in peroxo binding geometry from μ-η^1:η^1 to μ-η^1:η^2.

DOI: 10.1021/ja511649n
J. Am. Chem. Soc. 2015, 137, 1608−1617

Table 3. Spectroscopic Parameters of Synthetic Nonheme High-Spin Iron-Peroxo Complexes

complex[a]	λ_{max} (nm)	ε (M^{-1} cm^{-1})	ν (O−O) (cm^{-1})	J (cm^{-1})	δ (ΔE_Q) (mm s^{-1})	refs
$[(TMC)Fe^{III}(\eta^1\text{-}OOH)]^2$	500 (sh)	450	870		0.51 (0.2)	37
$[Fe_2(Tp^{iPr_2})_2(O_2CR)_2(\mu\text{-}\eta^1\text{:}\eta^1\text{-}O_2)]$	694	2650	888	66	0.66 (1.40)	20
$Fe^{III}(\mu\text{-}O)(\mu\text{-}\eta^1\text{:}\eta^1\text{-}O_2^{2-})Fe^{III}$	577−650	1200−1500	830−853	≥110	0.53−0.55 (1.43−1.68)	23,34,67−69
$Fe^{III}(\mu\text{-}OR)(\mu\text{-}\eta^1\text{:}\eta^1\text{-}O_2^{2-})Fe^{III}$	588−730	1500−3000	884−908	60−80	0.50−0.57 (0.96−1.35)	23,35,69
$[(py)_2Fe^{II}_2(dxlCO_2)_4(O_2)]$	500−550	1100	822	≈30(5)	0.65 (1.27) 0.52 (0.71)	57
nonheme $Fe^{III}(\eta^2\text{-}O_2^{2-})$	520−835	500−650	816−827		0.58−0.67 (0.6−1.4)	37,65,66,70,71
$(TMC)Fe^{III}(\mu\text{-}\eta^2\text{:}\eta^2\text{-}O_2^{2-})(Sc^{III})$	525	780	807/799		0.47 (0.50)	65,66
$(heme)Fe^{III}(\mu\text{-}\eta^2\text{:}\eta^1\text{-}O_2)Cu^{II}$			788−808			62,72
$(heme)Fe^{III}(\mu\text{-}\eta^2\text{:}\eta^2\text{-}O_2)Cu^{II}$			747−767			62,72

[a]Abbreviations used: $dxlCO_2$ = 2,6-bis(2′,6′-dimethylbenzyl)-4-*tert*-butylbenzoate anion; py = pyridine; TMC, 1,4,8,11-tetramethylcyclam; Tp^{iPr_2} = hydridotris(3,5-diisopropylpyrazolyl)borate anion.

What advantage might this difference in peroxo binding mode provide CmlI, and by inference, AurF? Reactivity data suggest that the decay of both peroxo intermediates is affected by the nature of the amine substrate, with more electron-rich substrates affording faster rates of decay (Figure 4C, inset).[73] It is thus plausible for CmlI and AurF to initiate the oxidation of their arylamine substrates by simple electron transfer to the peroxo intermediate (Scheme 1), thereby avoiding having to form oxidants more powerful than required for the reaction and affording the active site better control of the reaction coordinate. Accordingly, this mechanism may account for the inability of CmlI to catalyze either aliphatic or aromatic hydroxylation reactions despite the fact that its active site can accommodate a wide range of substrates.

Scheme 1. Proposed Mechanism for the First Step in Arylamine Oxygenation by CmlI

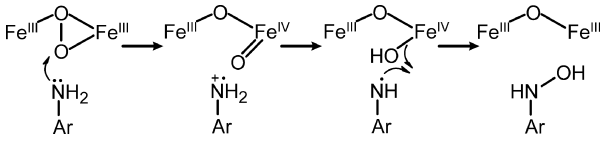

The mechanism shown in Scheme 1 would be a logical first step in the oxygenation of the arylamine substrate to the nitroaryl product. However, we have not detected the potential intermediate products, namely, the hydroxylamino- or nitroso-adducts of the NH_2-CAM substrate, during the reaction. Minor amounts of these intermediates were reported for reactions of both AurF and CmlI with their respective substrates in multiple turnover studies by Zhou and co-workers.[3,44] The single exponential time course for the reaction of NH_2-CAM with CmlI-peroxo suggests that, if these discrete intermediates are formed, their subsequent conversion to chloramphenicol is very fast. Recently, Krebs, Bollinger, and co-workers proposed that the AurF-peroxo adduct can react with the hydroxylamino-derivative of pAB by an interesting mechanism in which hydroxylation to form a dihydroxylamino-adduct is followed by two-electron, two-proton transfer to yield pNB and regenerate the AurF diferrous cluster.[28] Oxygen binding to the diferrous cluster would reform the AurF-peroxo adduct so that the hydroxylamino adduct is catalytically converted to the nitro adduct without net utilization of the peroxo adduct. While it is possible that CmlI follows this same mechanism, our results (Figure 3, inset) show that approximately three CmlI-peroxo complexes are required for each chloramphenicol produced from NH_2-CAM, favoring the stepwise oxidation mechanism.

A proposal for an unsymmetrically bound peroxo intermediate absorbing at 450 nm reminiscent of CmlI-peroxo was recently advanced for the enzyme aldehyde deformylating oxygenase (ADO) based on dissimilar Mössbauer parameters for the two ferric ions in the complex.[29] As we propose here for CmlI, the authors postulated that ADO-peroxo is the reactive species that directly attacks its long chain fatty aldehyde substrate. However, it was also proposed that the O−O bond cleavage reaction following formation of the initial hemiacetal species is promoted by transfer of one electron from an external donor.[74,75] No similar role for an external donor is evident in the efficient single turnover reaction of CmlI (Figure 4). Instead, electron transfer from the amine function of the substrate may serve this role of promoting O−O bond cleavage as illustrated in Scheme 1. An alternative mechanism for ADO was suggested by our recent study in which it was observed that the enzyme can hydroxylate the terminal methyl of the long-chain hydrocarbon formed as a product of long-chain aldehyde deformylation.[61] This implies that a high-valent species at the $Fe^{IV}Fe^{IV}$ oxidation state of MMO-Q is formed as a consequence of the O−O bond breaking reaction during deformylation. If this is the case, then an extra electron cannot be transferred to the peroxo intermediate in the ADO case. Similarly, electron transfer is not involved in the formation of MMO-Q prior to its reaction with methane.[10] This observation is in accord with the proposal made above in Scheme 1 that the difference in the type of substrate bond that can be oxygenated is a consequence of the availability of electrons to the peroxo intermediate.

Role of CmlI in Chloramphenicol Biosynthesis. Oxygenases in NRPS pathways have been shown to oxidize amino acid substrates in several modes, including: (a) prior to loading onto the peptidyl carrier protein (PCP) domain, (b) while the amino acid is tethered onto the PCP domain as a thioester, or (c) as a late-stage modification following release from the PCP.[76] We have shown in previous studies that L-pAPA β-hydroxylation during chloramphenicol biosynthesis catalyzed by the diiron monooxygenase CmlA proceeds exclusively by the second route.[2] The reactivity of CmlI-peroxo was interrogated in the current study using the free precursor substrate L-pAPA, L-pAPA appended onto the chloramphenicol NRPS CmlP PCP domain, NH_2-CAM, and other benzylamine substrates (Figure 4C, inset). The L-pAPA-loaded NRPS T-domain did not result in an appreciable enhancement of the peroxo decay rate, indicating that, unlike CmlA, CmlI does not perform oxidation chemistry on the S-acylated amino acid. The ability of CmlI-peroxo to fully convert NH_2-CAM to chloramphenicol was demonstrated by LC-MS studies (Figure S5) and is consistent with steady-state and whole cell turnover studies.[44]

DOI: 10.1021/ja511649n
J. Am. Chem. Soc. 2015, 137, 1608−1617

Thus, this reaction shows efficient six-electron oxidation of amine to a corresponding nitro derivative. The rate constant for CmlI-peroxo decay was significantly larger (~3×) for NH_2-CAM when compared to that of free L-pAPA, indicating that the installation of a nitro-group is enhanced by reduction of the L-pAPA carboxylate (which occurs during reductive cleavage from the NRPS) or installation of the dichloroacetyl group, or both. However, the efficient metabolism of NH_2-CAM observed here, considered together with earlier isotope feeding experiments used to order the modifications of CAM biosynthesis,[77,78] strongly suggests that CmlI functions as the last stage of CAM maturation as illustrated in Figure 8.

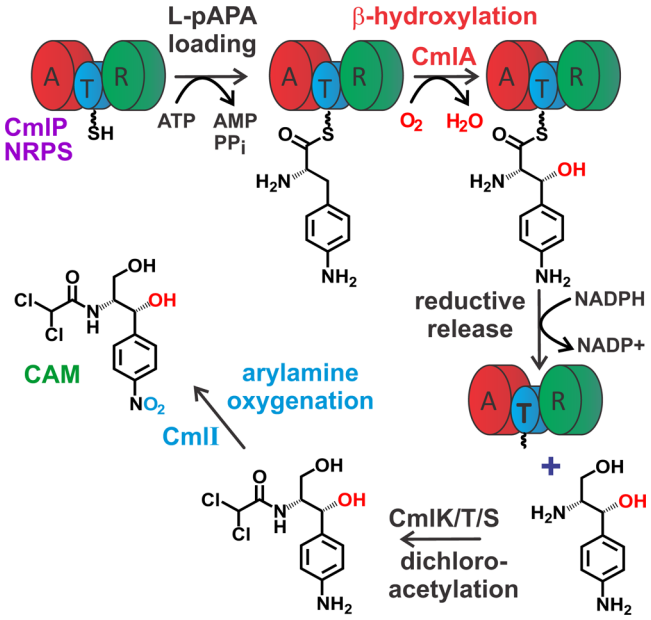

Figure 8. Role of CmlI in chloramphenicol biosynthesis.

■ ASSOCIATED CONTENT

Supporting Information

Detailed experimental procedures, characterizations of all compounds, and Figures S1–S7. This material is available free of charge via the Internet at http://pubs.acs.org.

■ AUTHOR INFORMATION

Corresponding Authors

*lipsc001@umn.edu
*emunck@cmu.edu
*larryque@umn.edu

Notes

The authors declare no competing financial interest.

■ ACKNOWLEDGMENTS

The authors acknowledge the financial support of this work from NIH GM100943 (to J.D.L.), NIH GM38767 (to L.Q.) and NSF CHE-1305111 (to E.M.). We thank Joseph Dalluge for assistance in mass spectral analysis.

■ REFERENCES

(1) Pilkington, S. J.; Dalton, H. *Methods Enzymol.* **1990**, *188*, 181.
(2) Makris, T. M.; Chakrabarti, M.; Münck, E.; Lipscomb, J. D. *Proc. Natl. Acad. Sci. U.S.A.* **2010**, *107*, 15391.
(3) Choi, Y. S.; Zhang, H.; Brunzelle, J. S.; Nair, S. K.; Zhao, H. *Proc. Natl. Acad. Sci. U.S.A.* **2008**, *105*, 6858.
(4) Vu, V. V.; Emerson, J. P.; Martinho, M.; Kim, Y. S.; Münck, E.; Park, M. H.; Que, L., Jr. *Proc. Natl. Acad. Sci. U.S.A.* **2009**, *106*, 14814.
(5) Mathevon, C.; Pierrel, F.; Oddou, J.-L.; Garcia-Serres, R.; Blondin, G.; Latour, J.-M.; Menage, S.; Gambarelli, S.; Fontecave, M.; Atta, M. *Proc. Natl. Acad. Sci. U.S.A.* **2007**, *104*, 13295.
(6) Wallar, B. J.; Lipscomb, J. D. *Chem. Rev.* **1996**, *96*, 2625.
(7) Tinberg, C. E.; Lippard, S. J. *Acc. Chem. Res.* **2011**, *44*, 280.
(8) Moenne-Loccoz, P.; Baldwin, J.; Ley, B. A.; Loehr, T. M.; Bollinger, J. M., Jr. *Biochemistry* **1998**, *37*, 14659.
(9) Beauvais, L. G.; Lippard, S. J. *J. Am. Chem. Soc.* **2005**, *127*, 7370.
(10) Lee, S.-K.; Nesheim, J. C.; Lipscomb, J. D. *J. Biol. Chem.* **1993**, *268*, 21569.
(11) Lee, S. K.; Fox, B. G.; Froland, W. A.; Lipscomb, J. D.; Münck, E. *J. Am. Chem. Soc.* **1993**, *115*, 6450.
(12) Shu, L.; Nesheim, J. C.; Kauffmann, K.; Münck, E.; Lipscomb, J. D.; Que, L., Jr. *Science* **1997**, *275*, 515.
(13) Bollinger, J. M., Jr.; Edmondson, D. E.; Huynh, B. H.; Filley, J.; Norton, J. R.; Stubbe, J. *Science* **1991**, *253*, 292.
(14) Baldwin, J.; Krebs, C.; Saleh, L.; Stelling, M.; Huynh, B. H.; Bollinger, J. M., Jr.; Riggs-Gelasco, P. *Biochemistry* **2003**, *42*, 13269.
(15) Broadwater, J. A.; Ai, J.; Loehr, T. M.; Sanders-Loehr, J.; Fox, B. G. *Biochemistry* **1998**, *37*, 14664.
(16) Bollinger, J. M., Jr.; Krebs, C.; Vicol, A.; Chen, S.; Ley, B. A.; Edmondson, D. E.; Huynh, B. H. *J. Am. Chem. Soc.* **1998**, *120*, 1094.
(17) Skulan, A. J.; Brunold, T. C.; Baldwin, J.; Saleh, L.; Bollinger, J. M., Jr.; Solomon, E. I. *J. Am. Chem. Soc.* **2004**, *126*, 8842.
(18) Broadwater, J. A.; Achim, C.; Münck, E.; Fox, B. G. *Biochemistry* **1999**, *38*, 12197.
(19) Valentine, A. M.; Stahl, S. S.; Lippard, S. J. *J. Am. Chem. Soc.* **1999**, *121*, 3876.
(20) Kitajima, N.; Tamura, N.; Amagai, H.; Fukui, H.; Moro-oka, Y.; Mizutani, Y.; Kitagawa, T.; Mathur, R.; Heerwegh, K.; Reed, C. A.; Randall, C. R.; Que, L., Jr.; Tatsumi, K. *J. Am. Chem. Soc.* **1994**, *116*, 9071.
(21) Kim, K.; Lippard, S. J. *J. Am. Chem. Soc.* **1996**, *118*, 4914.
(22) Dong, Y.; Yan, S.; Young, V. G., Jr.; Que, L., Jr. *Angew. Chem., Int. Ed.* **1996**, *35*, 618.
(23) Zhang, X.; Furutachi, H.; Fujinami, S.; Nagatomo, S.; Maeda, Y.; Watanabe, Y.; Kitagawa, T.; Suzuki, M. *J. Am. Chem. Soc.* **2005**, *127*, 826.
(24) Ookubo, T.; Sugimoto, H.; Nagayama, T.; Masuda, H.; Sato, T.; Tanaka, K.; Maeda, Y.; Okawa, H.; Hayashi, Y.; Uehara, A.; Suzuki, M. *J. Am. Chem. Soc.* **1996**, *118*, 701.
(25) Murray, L. J.; Naik, S. G.; Ortillo, D. O.; Garcia-Serres, R.; Lee, J. K.; Huynh, B. H.; Lippard, S. J. *J. Am. Chem. Soc.* **2007**, *129*, 14500.
(26) Song, W. J.; Lippard, S. J. *Biochemistry* **2011**, *50*, 5391.
(27) Korboukh, V. K.; Li, N.; Barr, E. W.; Bollinger, J. M., Jr.; Krebs, C. *J. Am. Chem. Soc.* **2009**, *131*, 13608.
(28) Li, N.; Korboukh, V. K.; Krebs, C.; Bollinger, J. M., Jr. *Proc. Natl. Acad. Sci. U.S.A.* **2010**, *107*, 15722.
(29) Pandelia, M. E.; Li, N.; Noergaard, H.; Warui, D. M.; Rajakovich, L. J.; Chang, W.-c.; Booker, S. J.; Krebs, C.; Bollinger, J. M., Jr. *J. Am. Chem. Soc.* **2013**, *135*, 15801.
(30) Saleh, L.; Krebs, C.; Ley, B. A.; Naik, S.; Huynh, B. H.; Bollinger, J. M., Jr. *Biochemistry* **2004**, *43*, 5953.
(31) Que, L., Jr.; Tolman, W. B. *Angew. Chem., Int. Ed.* **2002**, *41*, 1114.
(32) Girerd, J.-J.; Banse, F.; Simaan, A. J. *Struct. Bonding (Berlin)* **2000**, *97*, 145.
(33) Moenne-Loccoz, P.; Krebs, C.; Herlihy, K.; Edmondson, D. E.; Theil, E. C.; Huynh, B. H.; Loehr, T. *Biochemistry* **1999**, *38*, 5290.
(34) Fiedler, A. T.; Shan, X.; Mehn, M. P.; Kaizer, J.; Torelli, S.; Frisch, J. R.; Kodera, M.; Que, L., Jr. *J. Phys. Chem. A* **2008**, *112*, 13037.
(35) Frisch, J. R.; Vu, V. V.; Martinho, M.; Münck, E.; Que, L., Jr. *Inorg. Chem.* **2009**, *48*, 8325.

DOI: 10.1021/ja511649n
J. Am. Chem. Soc. 2015, 137, 1608–1617

(36) Roelfes, G.; Vrajmasu, V.; Chen, K.; Ho, R. Y. N.; Rohde, J.-U.; Zondervan, C.; la Crois, R. M.; Schudde, E. P.; Lutz, M.; Spek, A. L.; Hage, R.; Feringa, B. L.; Münck, E.; Que, L., Jr. *Inorg. Chem.* **2003**, *42*, 2639.
(37) Li, F.; Meier, K. K.; Cranswick, M. A.; Chakrabarti, M.; Van Heuvelen, K. M.; Münck, E.; Que, L., Jr. *J. Am. Chem. Soc.* **2011**, *133*, 7256.
(38) Mirica, L. M.; Ottenwaelder, X.; Stack, T. D. P. *Chem. Rev.* **2004**, *104*, 1013.
(39) Mathe, C.; Mattioli, T. A.; Horner, O.; Lombard, M.; Latour, J.-M.; Fontecave, M.; Niviere, V. *J. Am. Chem. Soc.* **2002**, *124*, 4966.
(40) Kitajima, N.; Moro-oka, Y. *Chem. Rev.* **1994**, *94*, 737.
(41) He, J.; Hertweck, C. *J. Am. Chem. Soc.* **2004**, *126*, 3694.
(42) Simurdiak, M.; Lee, J.; Zhao, H. *ChemBioChem* **2006**, *7*, 1169.
(43) He, J.; Magarvey, N.; Piraee, M.; Vining, L. C. *Microbiology* **2001**, *147*, 2817.
(44) Lu, H. G.; Chanco, E.; Zhao, H. M. *Tetrahedron* **2012**, *68*, 7651.
(45) Elango, N.; Radhakrishnan, R.; Froland, W. A.; Wallar, B. J.; Earhart, C. A.; Lipscomb, J. D.; Ohlendorf, D. H. *Protein Sci.* **1997**, *6*, 556.
(46) Rosenzweig, A. C.; Frederick, C. A.; Lippard, S. J.; Nordlund, P. *Nature* **1993**, *366*, 537.
(47) Pacholec, M.; Sello, J. K.; Walsh, C. T.; Thomas, M. G. *Org. Biomol. Chem.* **2007**, *5*, 1692.
(48) Vining, L. C.; Malik, V. S.; Westlake, D. W. S. *Lloydia* **1968**, *31*, 355.
(49) Dunham, W. R.; Harding, L. J.; Sands, R. H. *Eur. J. Biochem.* **1993**, *214*, 1.
(50) Dibar-Ure, M. C.; Flinn, P. A. In *Mössbauer Effect Methodology*; Gruverman, I. G., Ed.; Plenum Press: New York, 1971; Vol. 7, pp 245−262.
(51) Banerjee, R.; Meier, K. K.; Münck, E.; Lipscomb, J. D. *Biochemistry* **2013**, *52*, 4331.
(52) Rosenzweig, A. C.; Nordlund, P.; Takahara, P. M.; Frederick, C. A.; Lippard, S. J. *Chem. Biol.* **1995**, *2*, 409.
(53) Voegtli, W. C.; Khidekel, N.; Baldwin, J.; Ley, B. A.; Bollinger, J. M., Jr.; Rosenzweig, A. C. *J. Am. Chem. Soc.* **2000**, *122*, 3255.
(54) Andersson, M. E.; Hoegbom, M.; Rinaldo-Matthis, A.; Andersson, K. K.; Sjoeberg, B.-M.; Nordlund, P. *J. Am. Chem. Soc.* **1999**, *121*, 2346.
(55) Boal, A. K.; Cotruvo, J. A., Jr.; Stubbe, J.; Rosenzweig, A. C. *Science* **2010**, *329*, 1526.
(56) Ambundo, E. A.; Friesner, R. A.; Lippard, S. J. *J. Am. Chem. Soc.* **2002**, *124*, 8770.
(57) Chavez, F. A.; Ho, R. Y. N.; Pink, M.; Young, V. G., Jr.; Kryatov, S. V.; Rybak-Akimova, E. V.; Andres, H.; Münck, E.; Que, L., Jr.; Tolman, W. B. *Angew. Chem.* **2002**, *41*, 149.
(58) Liu, K. E.; Valentine, A. M.; Wang, D. L.; Huynh, B. H.; Edmondson, D. E.; Salifoglou, A.; Lippard, S. J. *J. Am. Chem. Soc.* **1995**, *117*, 10174.
(59) Krebs, C.; Bollinger, J. M., Jr.; Theil, E. C.; Huynh, B. H. *J. Biol. Inorg. Chem.* **2002**, *7*, 863.
(60) Hwang, J.; Krebs, C.; Huynh, B. H.; Edmondson, D. E.; Theil, E. C.; Penner-Hahn, J. E. *Science* **2000**, *287*, 122.
(61) Aukema, K. G.; Makris, T. M.; Stoian, S. A.; Richman, J. E.; Münck, E.; Lipscomb, J. D.; Wackett, L. P. *ACS Catal.* **2013**, *3*, 2228.
(62) Chufan, E. E.; Puiu, S. C.; Karlin, K. D. *Acc. Chem. Res.* **2007**, *40*, 563.
(63) Naruta, Y.; Sasaki, T.; Tani, F.; Tachi, Y.; Kawato, N.; Nakamura, N. *J. Inorg. Biochem.* **2001**, *83*, 239.
(64) Lewis, E. A.; Tolman, W. B. *Chem. Rev.* **2004**, *104*, 1047.
(65) Li, F.; Van Heuvelen, K. M.; Meier, K. K.; Münck, E.; Que, L., Jr. *J. Am. Chem. Soc.* **2013**, *135*, 10198.
(66) Lee, Y.-M.; Bang, S.; Kim, Y. M.; Cho, J.; Hong, S.; Nomura, T.; Ogura, T.; Troeppner, O.; Ivanovic-Burmazovic, I.; Sarangi, R.; Fukuzumi, S.; Nam, W. *Chem. Sci.* **2013**, *4*, 3917.
(67) Dong, Y.; Zang, Y.; Kauffmann, K.; Shu, L.; Wilkinson, E. C.; Münck, E.; Que, L., Jr. *J. Am. Chem. Soc.* **1997**, *119*, 12683.
(68) Kodera, M.; Kano, K. *Bull. Chem. Soc. Jpn.* **2007**, *80*, 662.
(69) Cranswick, M. A.; Meier, K. K.; Shan, X.; Stubna, A.; Kaizer, J.; Mehn, M. P.; Münck, E.; Que, L., Jr. *Inorg. Chem.* **2012**, *51*, 10417.
(70) Costas, M.; Mehn, M. P.; Jensen, M. P.; Que, L., Jr. *Chem. Rev.* **2004**, *104*, 939.
(71) Cho, J.; Jeon, S.; Wilson, S. A.; Liu, L. V.; Kang, E. A.; Braymer, J. J.; Lim, M. H.; Hedman, B.; Hodgson, K. O.; Valentine, J. S.; Solomon, E. I.; Nam, W. *Nature* **2011**, *478*, 502.
(72) Halime, Z.; Kieber-Emmons, M. T.; Qayyum, M. F.; Mondal, B.; Gandhi, T.; Puiu, S. C.; Chufan, E. E.; Sarjeant, A. A. N.; Hodgson, K. O.; Hedman, B.; Solomon, E. I.; Karlin, K. D. *Inorg. Chem.* **2010**, *49*, 3629.
(73) Platter, E.; Lawson, M.; Marsh, C.; Sazinsky, M. H. *Arch. Biochem. Biophys.* **2011**, *508*, 39.
(74) Li, N.; Norgaard, H.; Warui, D. M.; Booker, S. J.; Krebs, C.; Bollinger, J. M., Jr. *J. Am. Chem. Soc.* **2011**, *133*, 6158.
(75) Paul, B.; Das, D.; Ellington, B.; Marsh, E. N. G. *J. Am. Chem. Soc.* **2013**, *135*, 5234.
(76) Süssmuth, R. D.; Pelzer, S.; Nicholson, G.; Walk, T.; Wohlleben, W.; Jung, G. *Angew. Chem., Int. Ed.* **1999**, *38*, 1976.
(77) McGrath, R. M.; Siddiqueullah, M.; Vining, L. C.; Sala, F.; Westlake, D. W. S. *Biochem. Biophys. Res. Commun.* **1967**, *29*, 576.
(78) Westlake, D. W. S.; Vining, L. C. *Biotechnol. Bioeng.* **1969**, *11*, 1125.

DOI: 10.1021/ja511649n
J. Am. Chem. Soc. 2015, 137, 1608−1617